JOURNAL OF GEOPHYSICAL RESEARCH, VOL. 86, NO. A10, PAGES 8181–8198, SEPTEMBER 30, 1981

Measurements of Plasma Wave Spectra in Jupiter's Magnetosphere

F. L. SCARF

Space Sciences Department, TRW Defense & Space Systems Group, Redondo Beach, California 90278

D. A. GURNETT AND W. S. KURTH

Department of Physics & Astronomy, University of Iowa, Iowa City, Iowa 52242

The Voyager 1 and 2 plasma wave instruments had to be designed without direct knowledge of the intensities or spectral characteristics of waves in Jupiter's magnetosphere, the possible environmental problems at Jupiter, or the possible in-flight interference effects from Voyager subsystems. The wave instruments operated continuously during the 1979 Voyager encounters, and now we can assess in detail the performance of the receiver/spacecraft system within the magnetosphere of Jupiter. We present compressed plots of E field averages for all of the 16-channel spectrum analyzer data from the Voyager 1 and 2 magnetosphere traversals to provide an overall framework for the discussion. We illustrate the importance of considering peaks as well as averages by using 16-channel measurements from the first inbound and last outbound bow shock for Voyager 2. We also present selected wideband measurements from the waveform receivers to demonstrate how many important wave bursts are variable in times less than or comparable to the 4-s scan period of the 16-channel analyzer. These signal characteristics could not be determined by using the 16-channel analyzer data alone. In addition, we show how the continuous frequency coverage of the waveform data link provides extremely valuable information on the complex spectra of Jovian plasma waves. These wideband frames also lead to the identification of significant variable interference effects associated with the changing interaction between spacecraft subsystems and the Jupiter plasma environment.

INTRODUCTION

The knowledge that Jupiter has a large intrinsic magnetic field with a substantial population of energetic trapped electrons was derived many years ago from ground-based radio observations, and during the time that the Pioneer 10 and 11 missions were being designed, radio astronomers were able to provide considerable information on the field polarity, tilt, and offset, although these remote measurements gave little definitive information on the planetary field strength [*Carr and Gulkis,* 1969]. Similarly, while the radiometric observations were used to infer characteristics of energetic electrons in the inner magnetosphere [*Warwick,* 1970], the remote measurements did not yield any direct information about the fluxes of lower-energy electrons, the distributions of ions, the mechanisms responsible for charged particle acceleration and transport, or the dynamical phenomena of importance in the outer magnetosphere of Jupiter. Nevertheless, improved estimates of potential radiation damage effects were needed during the early phases of Voyager mission planning, and this requirement stimulated the development of detailed theoretical plasma physics models for outer planet magnetospheres. *Brice* [1972], *Thorne and Coroniti* [1972], and *Kennel* [1972] developed dynamical models with whistler mode instabilities that would control the dynamics of the Jupiter radiation belt and lead to stable trapping limits for electrons. These plasma physics calculations were then generalized to obtain early estimates of total radiation doses and peak fluences.

Although Pioneer 10 carried no specific instrumentation for magnetospheric plasma physics, the 1973 encounter data clearly showed that some kind of equatorial plasma sheet was associated with significant inflation of the magnetic field [*Smith et al.,* 1974; *Frank et al.,* 1976], that whistler mode waves had to be responsible for the observed electron pitch-angle distributions and trapped flux profiles [*Coroniti,* 1975], and that very strong acceleration processes had to be operative within the magnetosphere (see, for instance, the Pioneer 10, 11 summary by *Goertz* [1976]). The knowledge that Jupiter's magnetosphere contained energetic plasma led to additional speculation that some Pioneer 10 anomalies might have been associated with differential charging of the spacecraft [*Scarf,* 1975, 1976, 1977], and this suggested that Voyager needed a sheath-independent plasma density determination of the type associated with measurement of the cutoff frequency for trapped radio waves [*Gurnett and Shaw,* 1973].

Approval for the inclusion of a plasma wave investigation on Voyager came in July 1974, and the detailed design effort started shortly thereafter; however, this task had to be carried out with no real knowledge of the conditions to be encountered at Jupiter. That is, although the Pioneer 10 energetic electron data already suggested that strong whistler mode waves would be found in the inner magnetosphere, the interpretation did not lead to precise predictions about the wave amplitudes. Moreover, the available predictions involved amplitude estimates for magnetic components, and the associated wave electric fields would have additional amplitude uncertainties associated with possible variations in the wave index of refraction. In mid-1974, there were also no reliable estimates of inner magnetosphere wave amplitudes for other modes (such as ion cyclotron waves, ion acoustic waves, upper hybrid emissions, etc.), and there was no knowledge at all about plasma wave activity in the outer magnetosphere, the tail region, or the distant solar wind. Beside questions about sensitivity limits or saturation problems, there were serious uncertainties involving time variability for the Jovian plasma waves; this impacted the instrument design in terms of temporal sequencing requirements. Other questions of importance involved the effects of interference from the Voyager 2.4-kHz power supply and the effects of spacecraft charging on the plasma wave system, which necessarily used nongrounded metallic elements as electric field sensors.

Copyright © 1981 by the American Geophysical Union.

Paper number 80A1516.
0148-0227/81/080A-1516$01.00

The Voyager wave instruments operated continuously and successfully during the 1979 encounters with Jupiter, and the initial scientific results were discussed in the preliminary reports [*Scarf et al.*, 1979*a*; *Gurnett et al.*, 1979*b*] and in a number of other recent publications. This report is concerned primarily with another general aspect of the encounters relating directly to the performance of the receiver/spacecraft system within the magnetosphere of Jupiter. In order to evaluate the full significance of those measurements that were achieved successfully, we must assess the variations in the in-flight threshold levels, the way in which any restrictions in instrument characteristics could affect the data base, and the ability of the analysis program to distinguish between true Jovian plasma waves and signals generated on the spacecraft.

This discussion starts with a brief summary of the Voyager plasma wave instrument characteristics and the planned mode of operation during encounter. We then present compressed plots of 96-s electric field averages for all of the 16-channel spectrum analyzer data from the Voyager 1 and 2 magnetosphere traversals in order to provide an overall framework for the discussion and to provide a gross comparison of the two encounters. We show that these profiles of average amplitudes are very useful for discussions of electromagnetic waves, such as continuum radiation, hiss, and kilometric radiation, but we illustrate the need for higher time resolution by using 16-channel measurements in the regions of the first and last regular bow shock crossings for Voyager 2. Although the Voyager 16-channel analyzer provides an instantaneous bandpass channel measurement only once every 4 seconds, it is evident that in relatively broad regions that have impulsive wave activity (such as near the bow shock), the analyzer gives reliable information on the peak and the average wave spectrum.

Each Voyager plasma wave instrument also has a wideband waveform receiver covering the range 50 Hz to about 14 kHz, and the remainder of this report is concerned with the output from the wideband data link within Jupiter's magnetosphere. We use selected color-coded frequency versus time displays to show the enormous information content of the wideband link, which can provide an electric field waveform measurement once every 35 microseconds. We discuss the two modes of wideband data acquisition that involve regular (preplanned) frames and so-called 'unshuttered' frames in which unscheduled wideband plasma wave frames were transmitted as substitutes for nonuseful imaging output.

The waveform measurements are used to evaluate the limitations of the multichannel analyzer output, and it is shown that many important wave bursts in Jupiter's magnetosphere were variable in times less than or comparable to the 4-s scan period of the 16-channel analyzer. These signal characteristics could not be determined by using the 16-channel data alone. We also show how the wideband observations lead to detailed understanding of wave-particle interactions within the Io plasma torus, and we demonstrate how they provide identification of significant variable interference effects associated with the changing interaction between spacecraft subsystems and the Jupiter plasma environment.

The concluding section contains a postencounter assessment of the Voyager plasma wave instrument operation within Jupiter's magnetosphere. We note that the signal levels were always low enough so that it was never necessary to insert attenuators in order to shift the normal 100-db dynamic range. However, the detection of relatively low signal levels also means that it is not desirable to use a system with much less sensitivity than the Voyager one.

The Voyager analysis also conclusively establishes the great value of the waveform data in terms of mode identification, ability to analyze impulsive and/or dispersive events, ability to distinguish simultaneous multimode plasma wave emissions, and ability to separate varying interference signals from ambient plasma waves. Since only a very small fraction of the waveform data records have been processed to date, this means that many of the important Voyager plasma wave data analysis tasks for Jupiter are still ahead of us.

INSTRUMENTATION

Each of the Voyager plasma wave instruments utilizes a balanced electric dipole antenna with a 7-m effective length. The sensor output goes to a 16-channel analyzer covering the range from 10 Hz to 56 kHz and to a wideband receiver covering the range from 50 Hz up to about 14 kHz. The 16-channel analyzers do not sample continuously, since only two logarithmic compressors are used for the full spectral coverage, and there is no peak detection or sample-and-hold capability. At the highest general science telemetry rate in use during the planetary encounters, a full 16-channel spectral scan is completed once every 4 seconds.

The wideband receiver contains an automatic gain control (AGC) amplifier and a four-bit analog-to-digital converter to interface with the 115,200 bit per second Voyager high-rate telemetry link normally assigned to the imaging system. The output of the waveform amplifier is intermittently sampled at a rate of 28,800 words per second in 48-s intervals or frames.

A complete 48-s waveform frame has 800 successive 60 ms subsequences. For each of these there are 1600 consecutive waveform samples (in the first 55.6 ms) followed by a 4.4 ms interval with no plasma wave sampling. The 28,800 word per second sampling rate leads to a 35-μs time between samples, and this measure of the intrinsic time resolution of the Voyager wideband plasma wave system is marked on Figure 1. In order to avoid signal aliasing, the input circuit has a filter that rolls off strongly about 12 kHz, but very intense high- frequency signals could be detected up to the Nyquist frequency of 14.4 kHz. Other details of the instrument design and planetary science objectives are discussed in a report by *Scarf and Gurnett* [1977], and the top part of Figure 1 shows how the two analyzers cover the frequency range.

Figure 1 also contains a comparison of Voyager in-flight threshold levels with corresponding data from the ISEE 1 and 2 plasma wave instruments. The ISEE spacecraft were operating in the earth's magnetosphere in 1979, when the Voyagers encountered Jupiter, and it is of interest to contrast the capability for detection of weak plasma waves in the two magnetospheres. These threshold electric field curves are computed by assuming that in all cases the sensor effective length l_{eff} (7 m for Voyager 1 and 2, 107.5 m for ISEE 1, and 15 m for ISEE 2) is small in comparison with a half wavelength, so that $E_{\min} = \phi_{\min}/l_{\text{eff}}$, where $\phi_{\min}$ is the measured minimum voltage amplitude on the sensor. This means that the comparison of Figure 1 is valid as plotted only for those waves having $\lambda \gg 200$ m.

Even for these longer-wavelength oscillations, it can be seen that the Voyager sensitivity is excellent. For instance, in the 30–50-Hz range, the Voyager threshold is about a factor of 10 lower than that for ISEE 2, and approximately equal to the

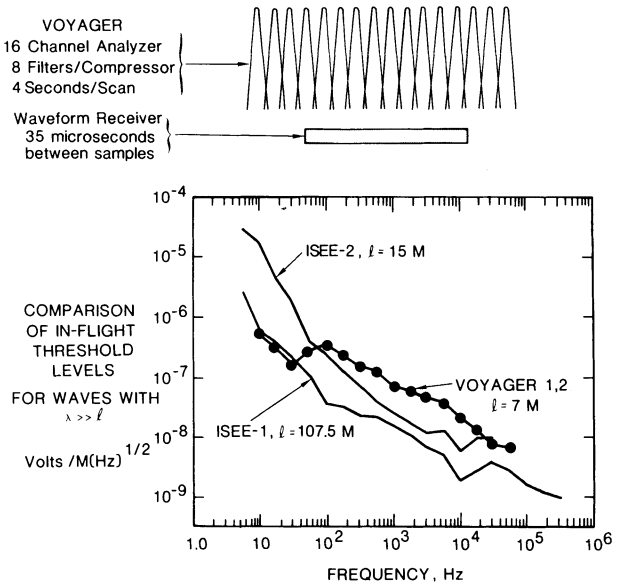

Fig. 1. Voyager plasma wave instrument characteristics. The frequency coverage is shown at the top, and the in-flight thresholds for Voyager 1 and 2 and ISEE 1 and 2 are compared at the bottom.

measured threshold for ISEE 1 [*Gurnett et al.*, 1978]. This result could never have been attained if the various in-flight thresholds were associated with detection of the same voltage noise signal from each of the spacecraft or from the essentially identical plasma wave preamplifier systems. In these cases we would expect to find $E_{\min} \times l_{\text{eff}} \approx$ constant, a result that is actually satisfied fairly well only in the narrow spectral range near 20 kHz.

The relation $E_{\min} \times l_{\text{eff}} \approx$ constant is also roughly satisfied for all frequencies above about 1 kHz, and this means that the exceptional aspect of the Voyager sensitivity develops only in the $f \leq 1$ kHz region. For instance, when we consider the differences in sensor effective length, we find that $\phi_{\min,\text{Voyager}} \approx \phi_{\min,\text{ISEE 1}}/14$ at $f = 10$ Hz. These low noise levels on Voyager are undoubtedly associated with the imposition of an electrostatic cleanliness specification leading to a Faraday shield around the spacecraft and to the absence of solar arrays, which frequently couple noise to the plasma; even before the launch of Voyager, *Scarf and Gurnett* [1977] discussed the good prospects for a quiet in-flight environment, such prospects being based on the unique characteristics of these RTG-powered spacecraft.

It should be recognized that the values for the threshold levels plotted in Figure 1 were derived by searching for the lowest readings in each channel, and this graph does not show the effects of several distinct sources of sporadic interference. In cruise it was determined that the plasma wave system detected: (a) enhanced noise in the 100-Hz to 311-Hz channels whenever the stepper motor of the low-energy charged particle instrument (LECP) was activated; (b) enhanced noise in the 560-Hz channel when a specific 400-Hz modulation tone was applied to one of the outer grids of the plasma probe (PLS); (c) low level 17-Hz and 56-Hz interference associated with operation of the planetary radio astronomy instrument (PRA); and (d) weak 300–500-Hz noise from the spacecraft gyros and the tape recorder. In addition we found that whenever the thrusters of the spacecraft altitude control system are fired, some of the three or four lowest-frequency channels of the plasma wave analyzer are likely to detect very strong but brief noise impulses. The cruise waveform measurements have allowed us to determine that this noise is a low-frequency impulse with peak intensity below 50 Hz and duration on the order of 1 to 2 s.

A different type of problem, involving the spacecraft analog to digital converters, developed on Voyager 2 shortly after launch. At 0045 SCET (spacecraft event time) on September 24, 1977, a circuit in the spacecraft flight data system failed, and this failure produced a nonlinearity in the telemetry interface for the upper eight channels of the 16-channel analyzer (1.0 kHz through 56 kHz). By comparing simultaneous Voyager 1 and 2 responses to solar radio bursts, we were able to recalibrate the flight data system interface for Voyager 2. This spacecraft problem has resulted in an elevation of the effective threshold level and a slight loss in the available dynamic range for the upper eight channels, but the overall effect on the performance of the Voyager 2 plasma wave instrument is a small one.

Spectrum Analyzer Measurements at Jupiter

The initial Voyager bow shock encounters occurred at 1434, February 28 (on Voyager 1) and 1619, July 2 (on Voyager 2). The final close-in crossings of the bow shock were at 1302, March 22 (on Voyager 1) and 1703, August 3 (on Voyager 2). The 'close-in' qualification refers to the fact that Voyager 2 reentered Jupiter's magnetosphere at least once in September 1979, but these more distant crossings are discussed in a separate paper [*Kurth et al.*, 1981].

Plate 1 shows 96-s E field averages for all the Voyager 1 and 2 16-channel measurements during the two Jupiter encounters, along with plots of the trajectories in planet-centered solar ecliptic coordinates. The frequency scales on the left side refer to the bandpass channel center frequencies, and the electron density values that correspond to equivalent electron plasma frequencies are shown on the right. (We use $f_p(\text{kHz}) = 9(N)^{1/2}$, with N in e/cm^3.) The vertical scale for each individual bandpass channel subpanel corresponds to an amplitude range of 5 orders of magnitude, and the arrows placed at the bottom of each encounter plot mark the multiple crossings of the Jovian bow shock.

The data presentations in Plate 1 are aligned so that the time for Voyager 1's closest approach (1200 on March 5, at $r = 4.9\ R_J$) is placed directly over the corresponding value for Voyager 2 (2230 on July 9, at $r = 10.1\ R_J$). Since the two time scales are the same and the distance scales are comparable, the different lengths of the two plots clearly show that the Voyager 2 flyby speed was significantly less than that of Voyager 1.

The Voyager 1 summary also contains an electron plasma frequency profile for $f \geq 100$ kHz. This double-peaked high-frequency curve, derived from observations by the Voyager planetary radio astronomy instrument (PRA), corresponds to the Voyager traversal through the Io plasma torus [*Warwick et al.*, 1979]. The Voyager 1 and 2 summary plots in Plate 1 also contain curves that represent our best estimates for the electron plasma frequency profile in regions for which f_p is less than about 5–10 kHz. Preliminary versions of sections of these curves were presented in several earlier reports [*Scarf et al.*, 1979*a*; *Gurnett et al.*, 1979*b*; *Barbosa et al.*, 1979; *Gurnett et al.*,

1980], and a companion paper in this issue [*Gurnett et al.*, 1981*a*] contains a discussion of Voyager electron density evaluations derived from some of the inbound wave measurements and an evaluation of the limitations and advantages of the various techniques.

Profiles of electron plasma frequency versus distance or time provide first-order information on the state of the magnetosphere, and the display in Plate 1 is specifically designed to indicate the extent of the changes in Jupiter's magnetosphere from one encounter to the next. This display also directly shows the differences in character between the inbound and outbound plasma density distributions.

Let us consider first the inbound legs. The Voyager 1 density profile was fairly regular within about 45 R_J, but for Voyager 2 the plasma density in the dayside magnetosphere was highly variable. Moreover, during the 24-hour interval ending at about 2000 on July 8, there was distinct evidence that Voyager 2 periodically emerged from a disk or sheet of high-density plasma into a low-density lobe region more commonly encountered on the nightside. We speculate that these dayside differences were associated with the fact that (a) Voyager 1 entered Jupiter's magnetosphere during a time when the peak solar wind pressure was unusually high [*Bridge et al.*, 1979*a*], and that (b) Voyager 2 was inbound at a relatively high magnetic latitude. *Gurnett et al.* [1979*b*] and *Kurth et al.* [1980*a*] showed that the differences in the observations of Jovian kilometric radiation (see the response in the 17.8-kHz, 31-kHz, 56-kHz channels) could be explained in terms of the different approaches to the magnetic equatorial plane.

Significant information on the inner magnetosphere can also be obtained from compressed data displays such as those contained in Plate 1. For instance, the Voyager 1 panel shows a very pronounced double-peaked increase in the low-frequency wave levels on March 5, 1979, as the spacecraft entered the Io plasma torus shortly before closest approach and then reentered the torus on the outbound leg. *Scarf et al.* [1979*a*, *b*] showed that at least some of these smoothly varying wave enhancements corresponded to detection of intense whistler mode turbulence capable of precipitating large fluxes of low-energy electrons [see also, *Thorne and Tsurutani*, 1979; *Coroniti et al.*, 1980]. One very significant aspect of the display in Plate 1 concerns the ability to compare directly the corresponding observations from the two spacecraft. For instance, we note that during the Voyager 2 encounter, strong low-frequency plasma wave turbulence was observable within about 22 R_J, while on Voyager 1, corresponding wave emissions were apparently detected only within about 10 R_J. This result demonstrates that the inner magnetosphere (i.e., $10 \leq R < 22$ R_J) plasma and field characteristics were not the same in March and July of 1979, and it shows that comparison of the 16-channel averages is an important first-order tool for analysis of the dynamics.

On the nightside, both plots of 96-s averages clearly reveal the existence of a broad region with relatively uniform high density ($N_e \simeq 5 \times 10^{-3}$ to 10^{-2} cm^{-3}) beyond about 160 R_J, where the disklike plasma sheet terminates. *Gurnett et al.* [1980] examined Voyager 1 outbound data from 20 R_J to 185 R_J and Voyager 2 outbound data from 50 R_J to 185 R_J, and they referred to this broad high-density region as a boundary layer. Plate 1 shows that Voyager 2 actually had multiple entrances into this region over an additional 10-day period as the spacecraft moved from 185 R_J to 280 R_J. This result is compatible with the trajectory plot, which indicates that Voyager 2 should have remained in the tail-boundary region during this time.

The large number of encounters with the tail-boundary layer and the multiple entrances into the outer magnetosphere on the dayside show that Jupiter's magnetopause is frequently in motion and that the location of the boundary varies widely in response to presumed changes in solar wind pressure. This interpretation is supported by noting that the bow shock surface, which should stand off by a large and relatively fixed distance from the magnetopause (i.e., $R_{\text{bow shock}} \approx 1.4\ R_{\text{magnetopause}}$ near local noon, as discussed by *Dryer et al.* [1973]; *Dryer* [1974]), was frequently encountered very near to the magnetosphere boundary. For instance, the third inbound Voyager 1 shock crossing at $R \simeq 72$ R_J was followed by a magnetopause crossing at $R \simeq 67$ R_J, leading to $R_{\text{shock}}/R_{\text{magnetopause}} \simeq 1.07$, rather than an expected value near 1.4. A similar relation was found for the final inbound crossing on Voyager 2 ($R_{\text{shock}}/R_{\text{magnetopause}}$) $\simeq 66.5/62 \simeq 1.07$), and these considerations suggest that the external boundary surfaces were in motion. However, the final close-in Voyager 2 shock crossings at $R \sim 282$–283 R_J on August 3 were essentially adjacent to the previous magnetopause crossing (at $R = 280$ R_J), and it seems that consideration of boundary motion may not be enough to explain these observations. It is conceivable that interplanetary events suddenly placed Voyager 2 in the solar wind beyond 282–283 R_J, and there is some evidence from the Voyager 1 plasma wave instrument (at 5.95 AU) that the interplanetary medium was quite active during this period. During the first half of August 5, Voyager 1 detected extensive wave activity in the 100-Hz to 1.78-kHz channels, and just after 1600 on August 8, a shocklike enhancement was detected on Voyager 1.

Some of the deficiencies in the use of electric field averages are also clearly suggested by the plots in Plate 1. Specifically, the label 'bow shock traversals' points to a few of the 14 arrows at the bottom of the Voyager 1 plot, and there are another 12 arrows at the bottom of the Voyager 2 plot, but almost all of these symbols refer to barely perceptible changes in the E field averages. This illustrates the fact that many very important wave-particle interactions involve plasma waves that have such impulsive characteristics that the signals are not at all adequately represented in an average plot.

Several of the initial Voyager 1 reports contained unaveraged wave profiles at the inbound bow shock crossings, and these figures clearly showed that strong bursts of electron plasma oscillations were detected in the 3.1- and 5.6-kHz channels upstream of very well-defined laminar shocks, which were characterized by the measurement of intense broadband plasma turbulence in thin layers. *Scarf et al.* [1979*a*] demonstrated that the first Voyager 1 inbound shock boundary was crossed in 2–3 min. The third Voyager 1 shock crossing was even thinner, and here the strongest low frequency ($10\ \text{Hz} \leq f \leq 3$ kHz) wave activity was detected for only about 1 min [see *Scarf et al.*, 1979*c*, and Figure 1 of *Gurnett et al.*, 1981*b*]. Thus it is not surprising that the laminar shock characteristics are poorly represented in plots of 96-s averages.

It is perhaps more surprising that Plate 1 shows few details of the first inbound Voyager 2 shock crossing on July 2, since this was described by *Bridge et al.* [1979*b*] as an extended pulsation shock. The plasma probe team identified specific crossings near 1619, 1622, and 1643, but they also noted that extensive upstream oscillations with periods of the order of 5 min were evident in the plasma density and other parameters. Since the total bow shock crossing lasted for a time very long

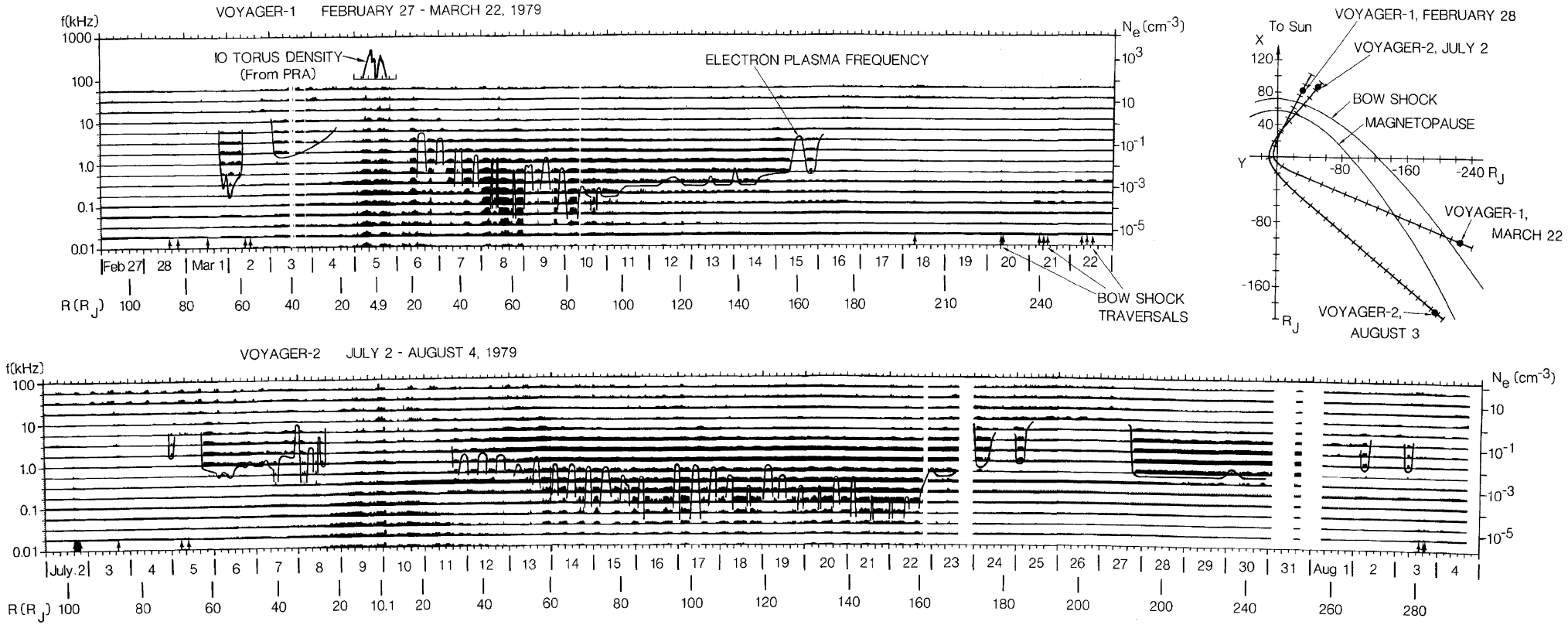

Plate 1. The 96-s averages of all Voyager 1 and 2 16-channel analyzer measurements within the magnetosphere of Jupiter. The arrows in the 10-Hz panels indicate times for bow shock crossings; the solid curves represent our best estimates of the electron plasma frequency profiles (see the scales on the right sides); and the vertical scale for each bandpass channel plot covers an amplitude range of 100 db.

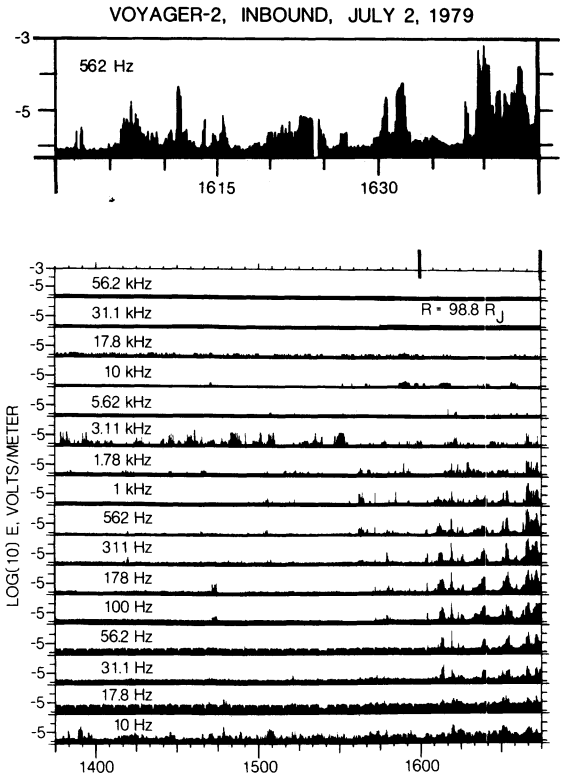

Fig. 2. Unaveraged E field measurements for the initial inbound Voyager 2 crossing of the bow shock. Interference effects from the spacecraft thrusters and the stepper motor of the low-energy charged-particle instrument have been removed. The expanded 562-Hz data segment in the upper panel illustrates how rapidly the wave amplitude changed.

compared to 96 s, the absence of a clear shock signature in Plate 1 would imply that all corresponding plasma wave levels were low or that the plasma wave activity was highly sporadic and impulsive.

Figure 2 shows the variations in the unaveraged plasma wave levels during the first Voyager 2 shock crossing. Here we have removed all samples containing interference effects associated with thruster firings and the LECP stepper motor, but all other data points are shown. The top panel of Figure 2 has a 1-hour profile of the wave activity in the 562-Hz channel, and the lower part of the figure shows the full set of the 16-channel measurements for a 3-hour interval. It is clear from this display that many intense bursts of low-frequency ($f < f_p \simeq 3.1$ kHz) plasma waves were detected after 1600, and the measurements near 1639 in the top panel show E field level changes going from a few microvolts per meter to almost 1 millivolt per meter in very short time intervals. This suggests that the plasma wave activity at the bow shock was indeed highly impulsive and that the once per 4 s scan time of the spectrum analyzer may, in fact, be quite inadequate for this type of wave activity.

Similar phenomena are illustrated in Figure 3, which shows the plasma wave data corresponding to the last Voyager 2 outbound bow shock crossing listed by *Bridge et al.* [1979*b*]. The bow shock on the magnetosphere flank is frequently weak and diffuse in the plasma wave data, and for the Voyager 1 outbound case this event appears to be relatively weak, and there is evidence for multiple crossings with the final outbound passage into the solar wind occurring at 1703. Here we have again tried to eliminate all effects of thruster firings and the LECP stepper motor, but the effort may not be completely successful. During three 10-min intervals, starting at 1619, 1707, and 1756, the LECP motor was stepped once per 6 s, and during these times, the interference effects in the 100, 178, and 311-Hz channels were so severe and persistent that when the spurious signals were removed, we may have removed relatively weak but potentially significant ambient plasma wave signals as well. In fact, as we shall discuss again below, several interference effects became progressively more severe during the Jupiter encounter, and Plate 1 shows that a number of other quasi-steady or repetitive wave enhancements started to affect the field averages just after the Voyager closest approach (for instance, the strong periodic ripples at 100, 178, and 311 Hz in the Voyager 1 outbound data, and the very intense 311-Hz signals on Voyager 2, which started soon after the long thruster firing at 0040 to 0155 on July 10). Despite these complications, the top panel in Figure 3 shows that even the weak outbound shock was clearly detectable in the unaveraged plasma wave data.

This discussion illustrates the need for high time resolution in order to detect and analyze impulsive signals and the corresponding need for high-frequency resolution in order to identify spacecraft signals and ambient plasma waves and to distinguish between them. However, since the 16-channel analyzer has only 4-s scan time and no sample-and-hold capability, the resulting time resolution is still not sufficient to carry out these tasks in many parts of the Jovian magnetosphere, and we turn to the wideband data.

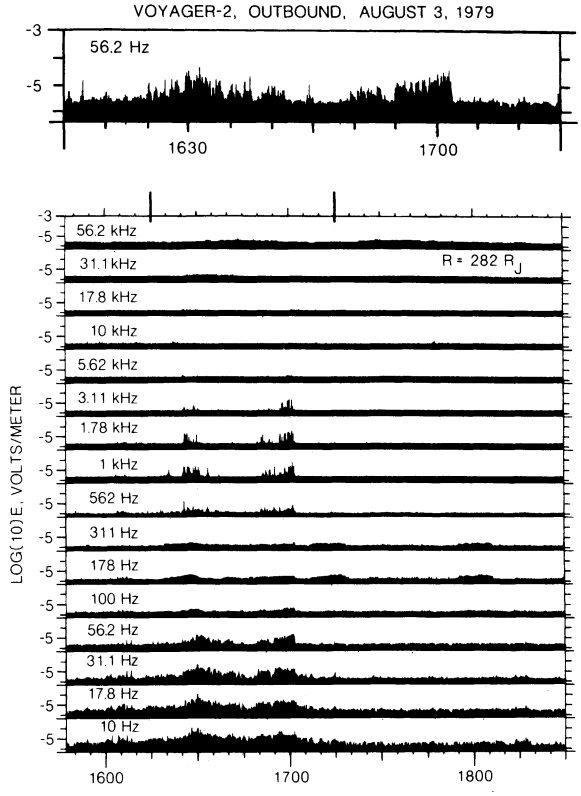

Fig. 3. Voyager 2 outbound measurements near the final regular crossing of the bow shock. As in Figure 2, the prominent interference effects have been removed.

TABLE 1. Number of Plasma Wave Wideband 48-s Frames per Day at Jupiter

Date Day	Scheduled Frame Count	Unshuttered Frame Count
	Voyager 1	
Feb 28 (59)*	10	430
Mar 1 (60)	14	1004
2 (61)	22	994
3 (62)	3	725
4 (63)	15	682
5 (64)	13	309
6 (65)	16	741
7 (66)	1	1043
8 (67)	2	722
9 (68)	2	57
Mar 10 (69)	2	522
11 (70)	4	783
12 (71)	0	0
13 (72)	0	530
14 (73)	0	235
15 (74)	10	18
16 (75)	22	49
17 (76)	8	12
18 (77)	12	499
19 (78)	28	186
20 (79)	19	393
21 (80)	23	325
Mar 22 (81)†	12	0
Totals:	238	10,259
	Voyager 2	
Jul 2 (183)*	4	55
3 (184)	8	44
4 (185)	22	
5 (186)	25	111
6 (187)	23	360
7 (188)	12	289
8 (189)	6	133
9 (190)	12	112
Jul 10 (191)	0	9
11 (192)	147	7
12 (193)	63	0
13 (194)	0	0
14 (195)	0	0
15 (196)	29	14
16 (197)	0	0
17 (198)	30	0
18 (199)	30	0
19 (200)	29	0
Jul 20 (201) through† Aug 3 (215)	0	0
Totals:	440	1,134

* After first bow shock
† Before last bow shock

THE WIDEBAND DATA AT JUPITER

The PWS wideband data acquisition for the Jupiter encounters was carefully planned to give an average of about ten 48-s long frames per day within the magnetosphere, along with a single continuous 3-hour sequence on July 11, 1979, after Voyager 2 closest approach. However, shortly before Voyager 1 encounter, it became evident that a specific imaging sequencing plan could not be implemented, and this discovery led to an enormous increase in the number of PWS high rate frames.

The imaging plan that presented a problem involved stored commands that provided automatic sequencing between the wide-angle and narrow-angle cameras in successive 48-s intervals. This cyclic was accomodated in the Voyager command memory, and it was planned to open the shutter for each camera only when that camera was pointed in a useful direction. However, the 'unshuttered' camera frames produced signals that did not modulate the telemetry in a satisfactory way, and the PWS wideband output was used to replace the camera output for these sequences, leading to a great increase in the average PWS acquisition rate within the magnetosphere. Specifically, during the 56 days in March, July, and August of 1979, shown in Plate 1, the Voyager 1 and 2 plasma wave instruments were scheduled to acquire a total of 678 48-s-long wideband frames, which had continuous spectral information over the range 50 Hz to 14,400 Hz. However, because of the changes in spacecraft sequencing, 12,071 wideband frames were actually acquired within the magnetosphere. Table 1 contains a daily tabulation of the scheduled frame count and a list of the number of unshuttered frames per day.

The data records for the 678 scheduled wideband frames have all been sent to the plasma wave investigators, and we have also received tapes for a small number of the additional unshuttered frames. We can start to evaluate the scientific value of the wideband data by examining a few examples from the subset of records (approximately 3% of the total from data Table 1) that have already been processed. We use color-coded intensity scales (blue represents a weak signal; red represents a strong one) to construct color frequency-time diagrams. The color processing is done at JPL's Imaging Processing Laboratory, and Plates 2 and 3 illustrate the results for 480 s of Voyager 1 and 2 wideband data.

The top panel in Plate 2 shows ion acoustic waves detected on February 20, 1979, when Voyager 1 was at 198 R_J in the upstream solar wind. The extreme variability of the wave freqeuncy with time could not even be detected with the 4-s scan time of the 16-channel spectrum analyzer. This frequency-time diagram also clearly illustrates how the spacecraft power system produces interference at 2.4 kHz. Moreover, between 1831:25.5 and 1831:27.5 the diagram shows that the plasma wave instrument detected signals with $f_n = (2n + 1) \times 400$ Hz, $n = 1, 2, \ldots$. These brief interference tones are generated whenever one of the outer grids of the Voyager plasma probe is modulated in a certain mode.

The second panel in Plate 2 has a color version of the frequency-time diagram for the Voyager 1 crossing of the Jupiter bow shock already discussed *Scarf et al.* [1979*c*]. *Gurnett et al.* [1981*b*] have used the high time resolution of the wideband link to analyze scattering and spatial collapse in the structure of the upstream electron plasma oscillations, thought to be associated with electron beams coming from the shock.

The third panel contains trapped radio waves or continuum radiation. *Scarf et al.* [1979*a*] showed how these particular Voyager 1 wideband measurements were needed to provide an unambiguous evaluation of the changing value for f_p, and *Gurnett et al.* [1981*a*] discuss precise density determinations based on analysis of about 30 similar wideband frames on Voyager 1 and 2. This panel also shows a number of additional interference signals. The low-frequency ($f \simeq$ 100–200 Hz) noise bursts at 2036:42 and 2037:06 represent interference associated with the stepper motor of the LECP (low-energy charged-particle instrument). At this time the ambient plasma waves were intense (note that the 2.4-kHz power supply tone does not appear here; strong signals mask 2.4-kHz noise, and even stronger ones cause the action of the plasma

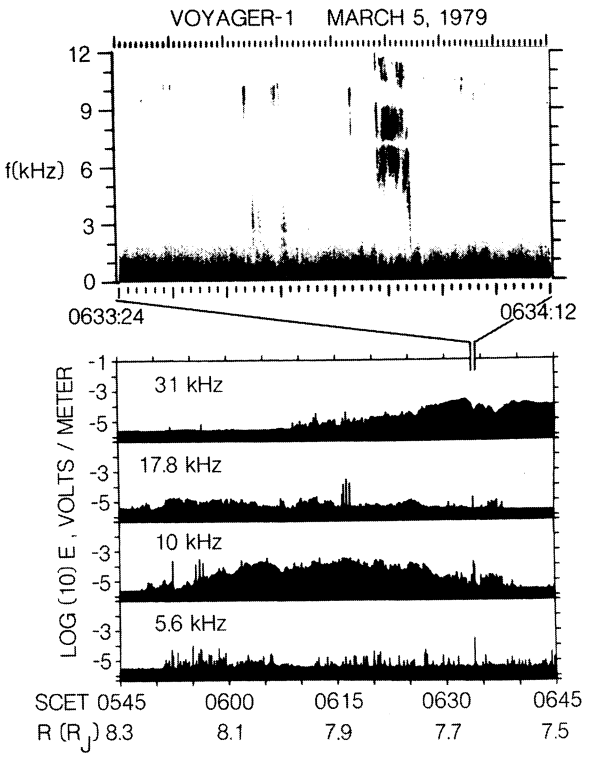

Fig. 4. Selected spectrum analyzer and waveform measurements near the Voyager 1 entrance into the Io plasma torus before periapsis. The frequency-time diagram shows that the isolated spikes in the bandpass channel actually represent brief but strong chorus emissions.

wave notch filter at 2.4 kHz to be evident), and the LECP noise was moderate.

The other low-frequency bursts in the third panel (for instance, the three spikes near 2036:57) are associated with another spacecraft noise source. The firing of the attitude control thrusters produces a characteristic intense low-frequency signal in the plasma wave antennas. We will return to the topics of the thruster firing noise and the LECP stepper motor interference later in the paper.

The bottom panel in Plate 2 shows Voyager 2 measurements of impulsive broadband electrostatic noise, with $f \lesssim$ 500 Hz, together with continuum radiation. Here, the high time resolution and the high-frequency resolution of the wideband data link both contribute in an essential way to the identification of the Jovian wave modes.

Plate 3 contains other important examples of Voyager 1 and 2 wideband frames. The top panel has an electrostatic emission at $3f_c^-/2$, where f_c^- is the electron gyrofrequency [*Kurth et al.*, 1980*b*], and the next panel has $f_c^-/2$ noise plus structured chorus. The chorus, half-gyrofrequency noise, and whistler mode hiss appear to be responsible for producing the Io torus aurora [*Scarf et al.*, 1979*b*; *Thorne and Tsurutani*, 1979; *Sandel et al.*, 1979; *Coroniti et al.*, 1980], and thus they represent very important equatorial wave emissions.

The third panel in Plate 3 is interesting because it displays a strong unidentified wave emission with some significant frequency variation over a very short time interval. As we shall see below (Figure 4), the existence of this wave might not even have been noted in the 16-channel data.

The bottom panel in Plate 3 shows continuum radiation below 2 kHz and Jovian kilometric radio emissions (JKR) near 10 kHz. The JKR frequency drift [*Kurth et al.*, 1979] is clearly evident here because the wideband data allows us to track small variations in wave frequency over short time intervals.

The large information content of the Voyager wideband data at Jupiter can best be appreciated by comparing the total number of data bits in Plates 1, 2, and 3. Plate 1 shows all of the 32 bit-per-second spectrum analyzer measurements for 58 days, and this involves a total of 1.6×10^8 bits. Although the measurements in Plates 2 and 3 cover only 480 s during this overall 58-day interval, these color frequency-time diagrams were made from data records containing a total of 5.1×10^7 bits, or about one third of the information content of Plate 1. Indeed, the 12,071 wideband frames listed in Table 1 involve a total of 6.2×10^{10} bits, and the intermittent wideband coverage in the magnetosphere thus involves measurements with almost 400 times the total data content provided by the spectrum analyzer.

The ability to study the entire plasma wave spectrum between 50 Hz and 14.4 kHz, with a time resolution of a fraction of a millisecond, is especially important when we detect waves that appear as impulses in the spectrum analyzer output, since isolated enhancements could be associated with bit errors, data dropouts, thruster firings, etc. Examples of such measurements are contained in the lower part of Figure 4, where the spectrum analyzer plot shows all observations in the four channels, 5.6 kHz to 31 kHz, for a 1-hour period when Voyager 1 crossed the magnetic equator as it entered the Io plasma torus. The initial broad 10-kHz wave enhancement between about 0555 and 0627 represents the main chorus emission sequence (see the second panel in Plate 3), and the isolated noise bursts near 0634 appear to be completely distinct. The digital records for the 5.6-kHz channel and the 17.8-kHz channel each show only a single noise spike (at 0633:52), and the two intense 10-kHz enhancements (at 0633:52 and at 0634:00) could be ignored as data dropouts. However, the broadband display at the top of Figure 4 clearly shows that these 'spikes' represent several strong but brief chorus emissions that followed the main chorus sequence.

Figure 5 contrasts some other examples of the broadband output with simultaneous measurements from the 16-channel analyzer. The bottom part of the figure contains Voyager 1 amplitude profiles for the upper eight channels over a 1-hour period that corresponds to the passage through the inner edge of the Io plasma torus. Between 0923 and 0926, the spectrum analyzer detected a number of isolated impulses, but the limited set of low rate observations did not provide enough information to describe the events or even determine whether they involved real signals or data anomalies. The 3-kHz bursts were detected in only two of the 16-channel scans (at 0923:45 and 0923:49), and the 10-kHz bursts were also detected in only two scans (at 0925:13 and 0925:17). However, the wideband measurements illustrate that at least two of the 'isolated' spikes that appeared in the spectrum analyzer output (see arrows) were intense, short-duration plasma wave emissions rather than interference bursts or data dropouts. The wideband data in Figure 5 also show that the plasma wave instrument detected intense undispersed noise spikes extending from below 2.4 kHz up to at least 12 kHz (see, for instance, the part of the frequency-time diagram for the interval 0924:18 to 0924:36). This result was common for the entire period when Voyager 1 was in the high-density part of the Io plasma torus, and a full discussion of possible interpretations will be presented in a separate report.

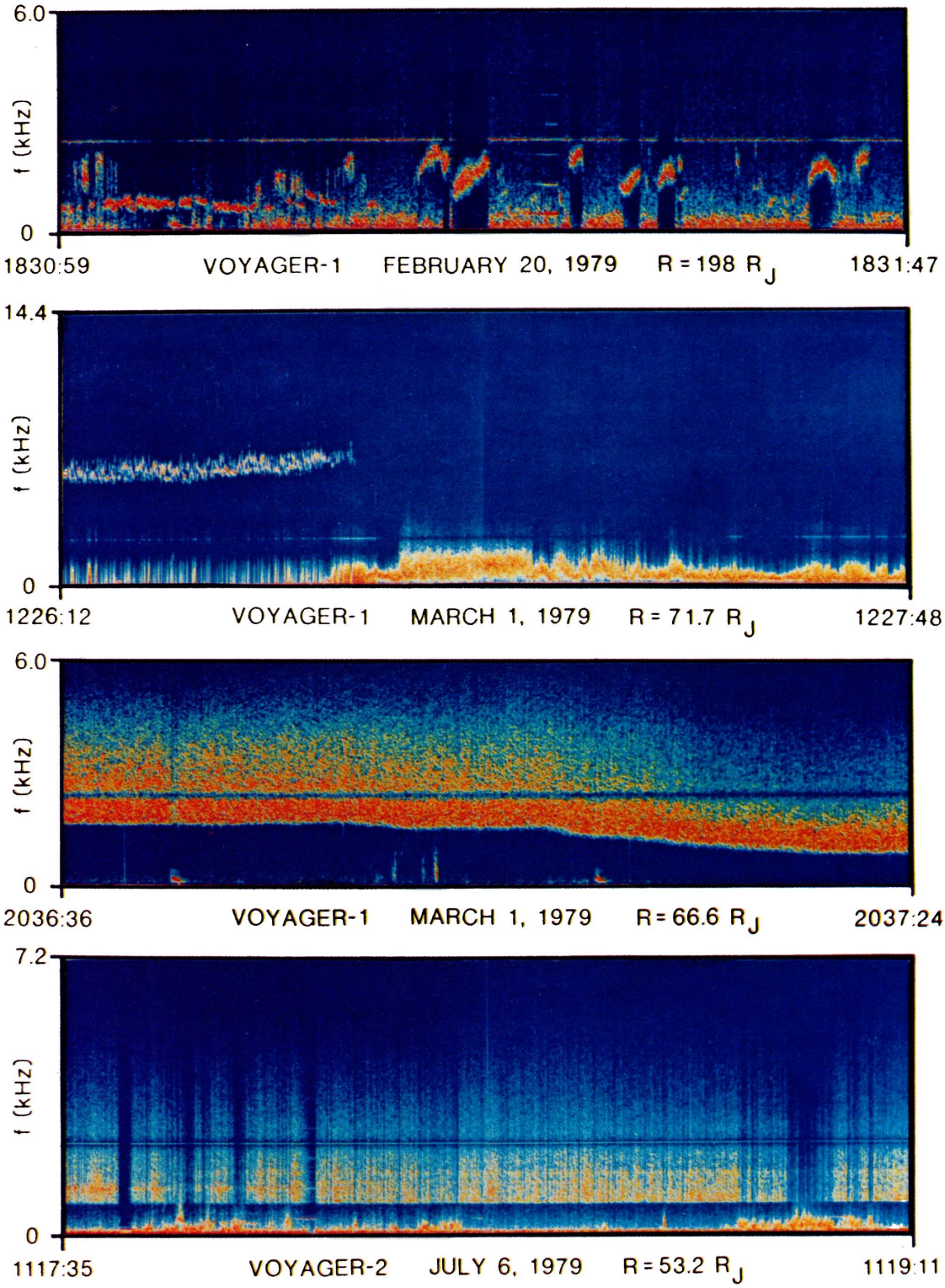

Plate 2. Color-coded frequency-time diagrams made up from the wideband 115,000 bit/second transmissions. The red tones correspond to the most intense signals, and the blue tones are the weakest ones. The top panel shows upstream ion acoustic waves, the second panel shows electron plasma oscillations and ion acoustic waves at an inbound bow shock crossing, the third panel shows continuum radiation, and the bottom panel has continuum radiation plus broadband electrostatic noise.

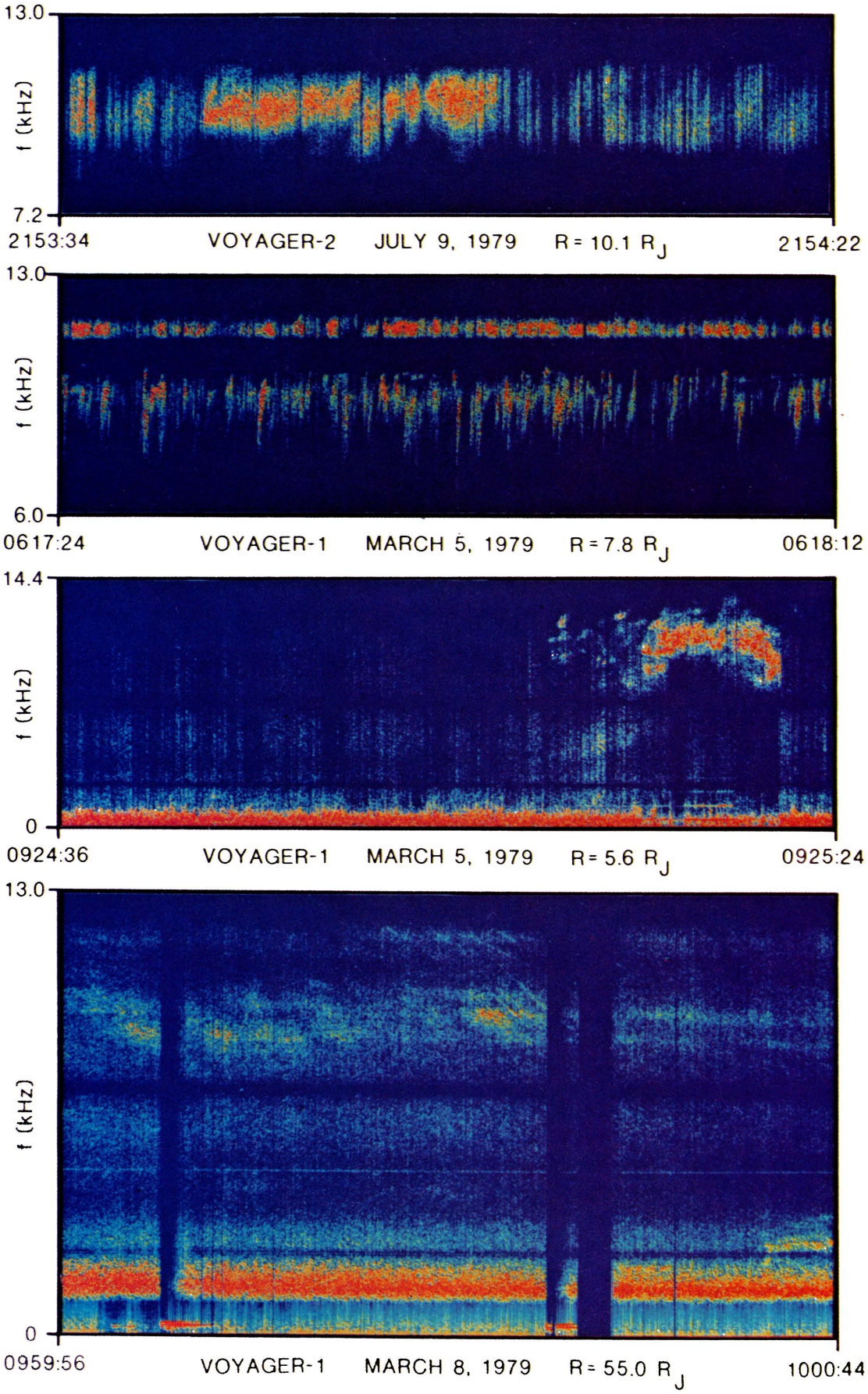

Plate 3. The top panel shows an emission at $3f_c/2$, the second panel has chorus plus an $f_c/2$ emission, the third panel has a strong but unidentified noise burst, and the bottom panel shows continuum radiation plus Jovian kilometric radiation with drifting structure.

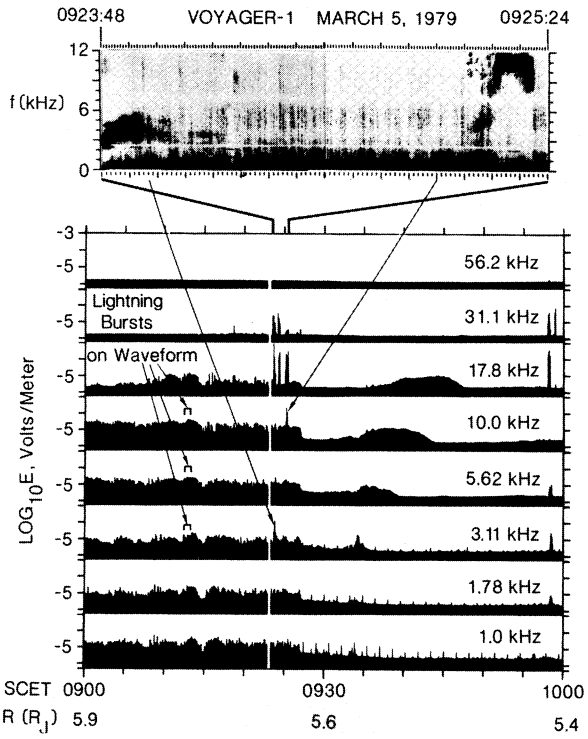

Fig. 5. Selected spectrum analyzer and waveform measurements near the Voyager 1 exit from the Io plasma torus before periapsis. Once again the frequency-time diagram shows that certain isolated spikes in the spectrum analyzer output represent real plasma waves. There is no evidence for discrete signals in the region near 0912–0913, as indicated.

The observations in Figure 5 can also be used to illustrate the limitations of the spectrum analyzer output for analysis of signals that last less than 4 s. It is noted on Figure 5 that lightning whistlers were detected during the 0912:20–0913:30 interval [see *Gurnett et al.*, 1979*a*], but no trace of these signals appears on the bandpass channel output. However, Figure 6 clearly shows the lightning whistlers, and *Menietti and Gurnett* [1980] used measured dispersions to deduce the high-latitude plasma density distribution and to place a bound on the electron temperature in the Io torus.

It is evident that wideband data at Jupiter represent an invaluable scientific resource for the plasma wave investigators and for the entire community interested in the dynamics of Jupiter's magnetosphere. However, since only a small fraction (≈3%) of the wideband data records at Jupiter have been processed to date, it is not possible to summarize the overall content of the Voyager plasma wave data set at this time.

Wave-Particle Interactions in the Inner Magnetosphere

Within the Io torus region, *Scarf et al.* [1979*a*] used Voyager 1 16-channel data to make an initial identification of what seemed to be a single broad low-frequency noise band having f_{max} less than the electron cyclotron frequency ($f_c = eB/2\pi mc$). They assumed that the waves were all whistler mode oscillations, and they suggested that the turbulence could pitch-angle scatter the trapped energetic electrons. Subsequently, *Scarf et al.* [1979*b*] and *Thorne and Tsurutani* [1979] quantitatively demonstrated that the associated pitch-angle diffusion rates would cause substantial precipitation of electrons with energies above about 100 keV. In addition, Thorne and Tsurutani noticed that an intensity peak at higher frequencies ($f \approx 10$ kHz) observed near 8 R_J on the Voyager 1 inbound pass might also be whistler mode noise, and *Scarf et al.* [1979*b*] pointed out that similar high-frequency waves capable of interacting with low-energy (1–10 keV) electrons were detected on the outbound pass.

Since the Voyager plasma wave investigation uses only a one-axis electric dipole antenna on a three-axis-stabilized spacecraft and since there is no magnetic wave sensor, the tentative whistler mode identification could not be verified by examining the ratio of the wave electric field to the magnetic component or by measuring the polarization or angular distribution of the wave field vectors. Without this type of supporting information, the conclusions about the electron pitch-angle diffusion rate, the magnitude of the precipitation flux, and the characteristics of the energy deposition in the atmosphere depend in crucial ways on other techniques for mode identification. Fortunately, the continuous frequency and time resolution of the waveform measurements generally provide the information needed to identify wave modes, as well as the spectral details needed for quantitative evaluation of the resulting wave-particle interactions.

The key to the analysis involves comparison of broadband wave data from Earth and Jupiter. Some aspects of the complexity and variable spectral structure of the Voyager plasma wave activity in the inner magnetosphere were already indicated in the wideband displays of Figures 4, 5, and 6, and Plate 2. These illustrations serve to demonstrate that, in fact, the measured turbulence cannot be described in terms of the initial concept of a single broadband spectrum having $f < f_c$. However, since some of the temporal and spectral features at Jupiter are very similar to those associated with familiar terrestrial plasma waves, the similarities allow us to be certain of our classification for these waves, and we identify the discrete lightning whistlers, the structured chorus bursts, and the narrow-band half-cyclotron frequency emissions as whistler mode oscillations [*Gurnett et al.*, 1979*a*; *Coroniti et al.*, 1980]. The mode identifications and the availability of complete spectral information from the waveform data then can be used to carry out precise evaluations of the pitch-angle diffusion effects for a range of electron energies.

In order to illustrate the analysis techniques, we consider the variety of whistler mode waves detected during the passage through the Io torus. The left side of Figure 7 has short sections of frequency-time diagrams taken from the more ex-

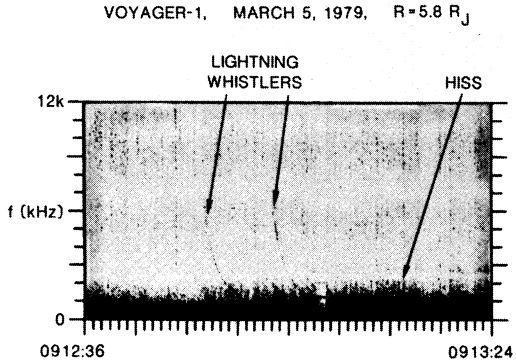

Fig. 6. Frequency-time diagram showing that lightning whistlers were detected in the waveform data near 0913.

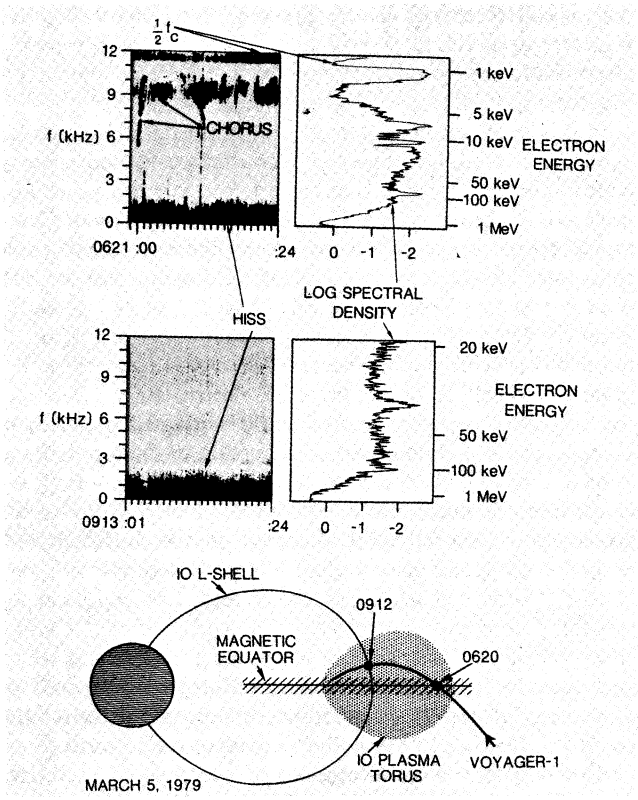

Fig. 7. Electron cyclotron resonant interactions within the Io plasma torus. Voyager 1 frequency-time and frequency-spectral density diagrams for the Io L shell crossing (center) and the magnetic equator crossing (top) are presented along with the associated minimum resonant energy scales (right sides), as computed by using (1).

tensive displays of Plate 3 (panel 2) and Figure 6, and the labels point to the hiss, the chorus, and the $f_c/2$ emissions. The drawings on the right side show the relative spectral density as given by numerical analysis of the waveform data. In both cases the spectral densities represent averages of successive 1600-sample waveform sequences; the lower plot is a 10-sequence average from a 0.6-s-long interval near 0912:56 (see Figure 6), and the upper drawing is a 50-sequence (3-s) average from data taken near 0620:46 (see Plate 3). The frequency scales for the spectral density plots are the same as those for the frequency-time diagrams, and corresponding wave modes can be identified in both formats (the spectral density plots also clearly show the instrument notch filters at 2.4 and 7.2 kHz).

The whistler mode wave-particle interactions within the torus involve the Doppler-shifted cyclotron resonance, and for waves interacting with relativistic electrons, the resonance condition is

$$(f - \mathbf{k} \cdot \mathbf{v}/2\pi) = f_c\,(1 - v^2/c^2)^{1/2} \qquad (1)$$

Here, f is the wave frequency, $\mathbf{k}$ is the wave vector, $\mathbf{v}$ is electron velocity, and c is the speed of light [see, for instance, *Scarf et al.*, 1979*b*]. At any location, the wave vector and wave frequency are uniquely related by the expression for the whistler mode index of refraction n, and hence, any selected wave frequency is uniquely associated with a local value for a minimum electron speed that will yield resonance. Thus, at any point along the trajectory, we can use (1) and the expression for n to compute a resonant energy versus frequency transform that leads to an energy scale for both the frequency-time diagram and the related spectral density versus frequency plot.

Full discussions of these calculations for the Io torus traversal on March 5, 1979, are contained in the reports by *Scarf et al.* [1979*b*], *Thorne and Tsurutani* [1979], and *Coroniti et al.* [1980]. The appropriate electron energy scales for cyclotron resonance at the particular times 0620 and 0912 are shown on the right sides of the data panels in Figure 7, and these results clearly indicate how the features in the whistler wave spectrum selectively interact with well-defined subsets of the trapped electron population. For instance, the hiss band at 0912 was able to cause significant pitch-angle diffusion for electrons with $E \simeq 100$ keV to about 1 Mev, but at these high energies the associated precipitation could not be effective in stimulating auroral emissions. On the other hand, the chorus and $f_c/2$ modes detected near 0620 had to interact directly with electrons with $E \simeq 1$–5 keV, and *Coroniti et al.* [1980] showed that the associated precipitation flux could explain many characteristics of the observed auroral emissions. Thus the detailed analysis of the magnetospheric plasma wave measurements from the region near the Io orbit provides important information on the precipitation processes that directly affect the Jupiter atmosphere at high latitudes. The hiss detected throughout the Io torus region leads to loss of $E > 100$ keV electrons, which deposit their energies relatively low in the atmosphere, while the discrete higher-frequency waves detected near the magnetic equator lead to precipitation of the softer electrons, which do generate the auroral emissions.

The wideband data also help us to analyze electrostatic waves and the associated wave-particle interactions, but these waves have phase speeds comparable to or smaller than the magnetospheric corotation speed, and Doppler shifts complicate the interpretations. Let us consider the Voyager 2 wave measurements shown in the top panel of Plate 3. Here, B was 325 γ, f_c was 9.1 kHz, and *Kurth et al.* [1980*b*] classified this intense equatorial noise burst as one of the $(n + 1/2)f_c$ electrostatic wave emissions [*Kennel et al.*, 1970]. They noted that the terrestrial $3f_c/2$ emissions often occur close to f_c [*Shaw and Gurnett*, 1975], but they did not comment on the unusually wide bandwidth shown here ($\Delta f/f \simeq 0.2$ to 0.25) or the unusual vertical structure apparent in the top panel of Plate 3.

Let us consider the way in which the Doppler shift could affect the observations. The shortest wavelength $(n + 1/2)f_c$ oscillations have $kR_e \approx 1$, where $R_e = a_e/2\pi f_c$ is the electron Larmor radius and a_e is the electron thermal speed. These short wavelength oscillations can have large Doppler shifts, since $f' = f + k \cdot V/2\pi$ leads to

$$2\pi|\Delta f(\text{Doppler})|_{\max} \approx V/R_e \simeq 2\pi f_c\, V/a_e \qquad (2)$$

For $r \simeq 10\ R_J$ on Voyager 1, *Bagenal and Sullivan* [1981] showed that $V \simeq 0.8\ V$(corotation) $\simeq 100$ km/s, and they noted that $T_e \approx 10$ eV. These numbers give $a_e \simeq 2 \times 10^6$ m/s, $R_e \simeq 33$ m, and $\Delta f \simeq 1$ kHz, in fairly good agreement with the measured Voyager 2 bandwidth, as shown in Plate 3. It is thus possible to associate the frequency range with the presence of a range of values for the angle between k and V, or with waves having $kR_e \ll 1$; in either case, the Δf value would be small in comparison with $|\Delta f|_{\max}$, so that we could simultaneously detect waves with different Doppler shifts, leading to a set of vertical noise spikes, as shown.

The ion gyroharmonics will also experience Doppler shifts,

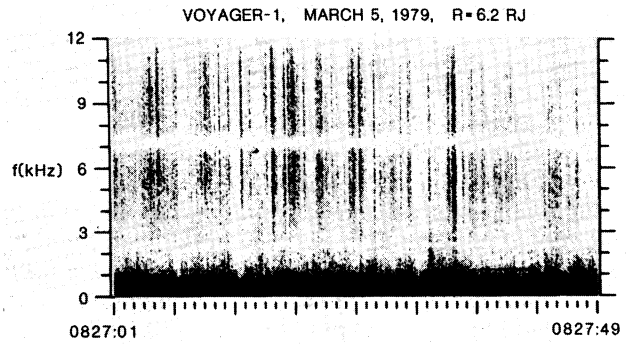

Fig. 8. Impulsive noise bursts detected within the Io plasma torus. These waves, which were commonly present in the torus region, might represent detection of Doppler-shifted ion acoustic waves.

but since f_c^+/a_i is at least a factor of $(1840)^{1/2}$ smaller than f_c/a_e, the effect will be much less. It is of interest to note, however, that at $r = 10\ R_J$, $N_e \simeq 40\ \text{cm}^{-3}$ [*Gurnett et al.*, 1981*a*], so that the Debye length λ_D is on the order of 3.7 m. Thus $2\pi\lambda_D \simeq 23$ m, and the peak Doppler shift for ion acoustic waves, which is approximately given by

$$\Delta f \simeq (k\lambda_D)Vf_p/a_e \approx Vf_p/a_e \quad (3)$$

turns out to be about 3 kHz.

In the middle of the Io torus, the corotation speed, the electron Larmor radius, and the Debye length are all smaller than they are at 10 R_J, and we find that, generally, the magnitude of the Doppler shift is considerably larger here. For instance, during the inbound crossing on Voyager 1, *Bagenal and Sullivan* [1981] found $V = V$(corotation = 75 km/s and $a_e = 1.3 \times 10^6$ m/s ($T_e = 5$ eV) at $L = 6$ (0900, March 5, 1979). Since f_c was 56 kHz at this location, the local electron Larmor radius was 3.8 m, leading to $|\Delta f|_{\max} \simeq 6$ kHz for $(n + 1/2)f_c$ waves. Once again, we can conclude that the electrostatic ion gyroharmonic modes with minimum wavelength on the order of the ion Larmor radius would have much smaller Doppler shift effects. However, in the inner torus region it can readily be shown that the extremely small Debye lengths and high corotation speeds lead to enormous Doppler shifts for ion acoustic waves. For example, at 0900 on March 5, 1979, *Warwick et al.* [1979] found $N_e \simeq 10^3\ \text{cm}^{-3}$, so that here $\lambda_D \simeq 0.53$ m and $(2\pi\lambda_D) \simeq 3.3$ m. When observed from a spacecraft moving at 75 km/s through the plasma, the frequency shift for this ion acoustic wave could be as high as 16 kHz.

These effects must be considered when we search for evidence of waves that could cause the enhanced ion pitch-angle diffusion first detected on Pioneer 10 and 11 [*Thomsen et al.*, 1977]. The Voyager LECP instrument also provided evidence for very severe ion losses within the Io plasma torus with a sharp transition to a loss-free region at $L \simeq 5.6$–5.7 [*Armstrong et al.*, 1981], and E. C. Stone et al. (private communication, 1980) reported detection of a very distinct inner boundary for losses of more energetic ions at the same location. The conventional ion loss theories [*Thomsen et al*, 1977; *Goertz*, 1980] involve pitch-angle diffusion caused by low-frequency, long-wavelength ion cyclotron waves, which would not involve significant Doppler shifts. Near closest approach on Voyager 1, the plasma wave instrument might possibly have detected weak evidence for these ion resonant waves in the 10-Hz and 17-Hz channels [see Figure 3 of *Scarf et al.*, 1979*b*]. However, this mode identification is necessarily inconclusive because the measured activity in the 10- and 17-Hz channels could represent detection of electromagnetic whistler mode waves or electrostatic ion gyroharmonics as well as electromagnetic ion cyclotron modes.

In this inner torus region the waveform data also provide evidence of Doppler-shifted ion acoustic waves which might contribute in a very significant way to ion loss processes. Figure 8 shows one promising Voyager 1 waveform example for a typical period in the Io torus when the chorus and $f_c/2$ emissions were absent. This frequency-time diagram has the customary hiss band below a few kilohertz, along with a large number of impulsive noise spikes. Broadbanded sequences of noise bursts with this appearance on a frequency-time diagram are generally associated with electrostatic modes, and the impulsive structure is frequently explained in terms of Doppler shifts, as in our earlier discussion of the top panel of Plate 3. Since the frequency span of each impulse in Figure 8 is less than the maximum computed Doppler shift for an ion acoustic wave, the full set of measurements are consistent with an ion sound identification. Plasma wave emissions with very similar wideband characteristics were detected beyond the terrestrial plasmapause on S^3-A, and *Anderson and Gurnett* [1973] speculated that these may have been ion acoustic waves generated by a high-β loss cone instability, as proposed by *Coroniti et al.* [1972]. A modified version of this instability could be operative in the hotter regions of the Io torus.

Although only a small number of wideband data frames from this region have been available for processing and inspection, we find that the structure illustrated in Figure 8 is more typical within the Io plasma torus than any other. The frequency-time diagrams in Figures 5 and 6 show many other examples of weaker undispersed or vertical impulses. Referring to the lower part of Figure 5, we note that the enhanced responses in the 1.0- to 17.8-kHz bandpass channels before about 0927 could represent essentially continuous detection of these broadbanded noise bursts. This possibility would imply that strong ion acoustic waves were present only up to 0927 and that the waves disappeared near $L = 5.6$ to 5.7, just when the pitch-angle scattering effects for the ions also disappeared, so that a connection between ion sound waves and ion precipitation would be indicated. Further detailed correlative studies are required to determine whether or not these speculations will turn out to be correct.

VARIABLE SPACECRAFT-PLASMA WAVE INTERACTIONS

During the extensive Voyager design and integration phases, concerns about the Jupiter radiation hazard, spacecraft charging, and electromagnetic and electrostatic interference were identified and addressed. At that time, the radiation problem was fairly well understood on the basis of Pioneer 10 and 11 data, but interpretations of Pioneer anomalies in terms of possible charging phenomena were quite speculative [*Fillius and McIlwain*, 1974; *Scarf*, 1975, 1976, 1977], and no information at all was available on the behavior of Voyager subsystems as noise sources in a changing and unknown plasma environment. *Scarf and Gurnett* [1977] noted that the attempt to impose an electrostatic cleanliness specification, the use of a balanced electric field dipole antenna, and the insertion of notch filters at 2.4 and 7.2 kHz would all serve to minimize interference effects, and the plasma wave input system was also modified to restrict the development of large potential differences between the floating antenna elements and the spacecraft ground.

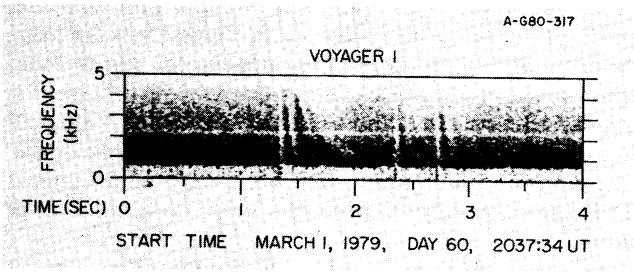

Fig. 9. The vertical spikes and echoes originating near 1.35, 2.35, and 2.7 s after the 2037:34 start time have sounds that resemble electrical discharges. These noise bursts are associated with thruster firings in energetic plasma regions, and we conjecture that the ionization products from the thrusters reduce large voltage differences.

It is important to study the actual variations in coupling between spacecraft subsystems and the Jovian plasma and wave environment because the full analysis must ultimately be used to remove all spurious interference signals and it is important to correct charged particle measurements for sheath effects. Completion of this study will require detailed multi-instrument correlations that are beyond the scope of the present report. However, it is possible to present here plasma wave evidence for some unexpected and significant anomalies and variations in spacecraft-plasma interactions.

The first evidence for local spacecraft-plasma interactions was obtained just after Voyager 1 first entered Jupiter's magnetosphere on March 1, 1979. As shown in the third panel of Plate 2, the electron density started to drop near 2037, and the plasma temperature rose into the 20–30-kV region [*Krimigis et al.*, 1979]; these changes would be likely to generate a sudden variation in spacecraft potential, with associated development of some differential charging, and this caused us to scrutinize the plasma wave data for possible evidence of discharges. The initial search involved audio analysis of the wideband data, and we immediately heard sounds resembling discharges or arcs. An expanded frequency-time diagram for one interesting period, which started 10 seconds after the end of the Plate 2 interval, is shown in Figure 9.

The discharge-type sounds are the vertical spikes and echoes starting near 1.35 s, 2.35 s, and 2.7 s after the 2037:34 start time of Figure 9. It is significant that all three of these spikes are associated with impulses extending down to very low frequencies. Our detailed analysis of the impulse timing suggests that all three of these noise spikes were actually associated with firing of the hydrazine thrusters, and our tentative interpretation is that the ionization products from the thrusters serve to discharge the large differential voltages that naturally developed on the nonequipotential Voyager surfaces, such as the large antenna dish and the scan platform calibration plate (these items, and others, did not satisfy the equipotential specification). Similar signals were detected on Voyager 1 and 2 in some post-encounter wideband frames, and we speculate that gases from the attitude control system served as electron sources that limited the development of dangerous differential charge states in the high-temperature regions of Jupiter's magnetosphere.

Another phenomenon that may have been associated with spacecraft charging involved the variation in the effect of the interference from the LECP stepper motor. The most rapid stepping sequence has the motor activated once every 6 s, with a 12-s gap following the seventh step [see *Krimigis et al.*, 1979, for details]. We found that while the normal 'thump' associated with this motion generally lasted on the order of 2 s or less (in the solar wind, in the magnetosheath, and in high-density plasma regions), the stepper motor produced severe and persistent ringing in parts of Jupiter's magnetosphere. Figure 10 shows some of this variability. The top panel illustrates the normal brief interference pattern, and the bottom two panels show the increasing persistence of the stepper motor noise pickup and the increasingly severe blanking action on the gain state of the plasma wave amplifier system. During parts of the tail encounter, the ringing lasted for more than 6 s, and the associated interference caused serious degradation of the wave data.

At present, we do not have a firm explanation for this variation in interference, but it seems likely that it is associated with direct excitation of oscillations by motion of the LECP instrument within the plasma sheath surrounding the Voyager spacecraft. However, since the timing of the stepper motor in-

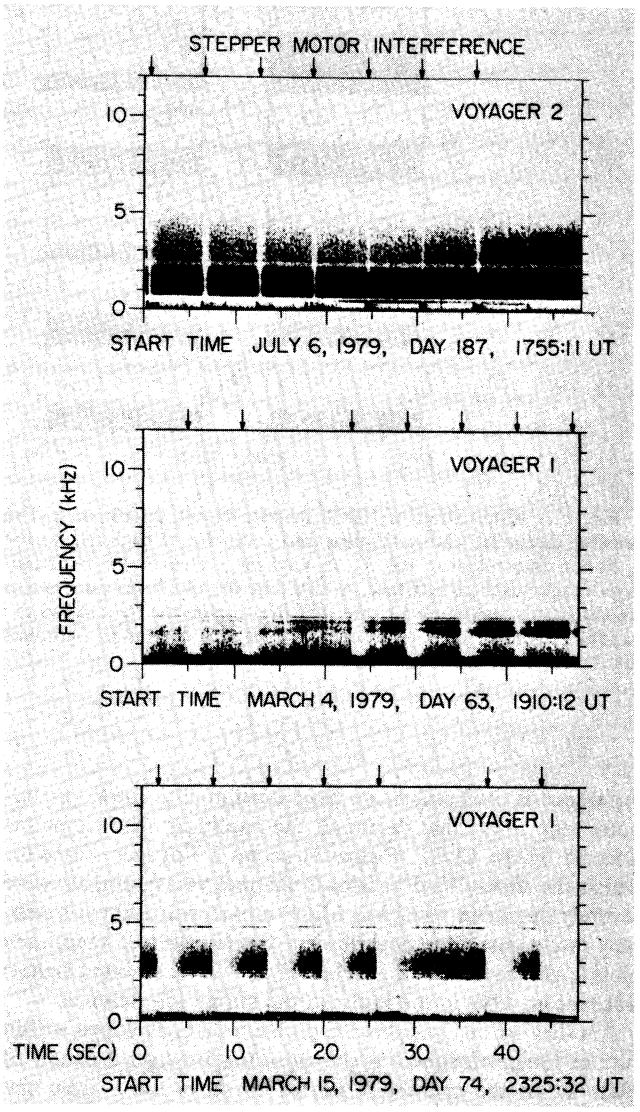

Fig. 10. Variation of LECP stepper motor interference. It appears likely that the motion triggers sheath oscillations that persist for a time that depends on the plasma conditions.

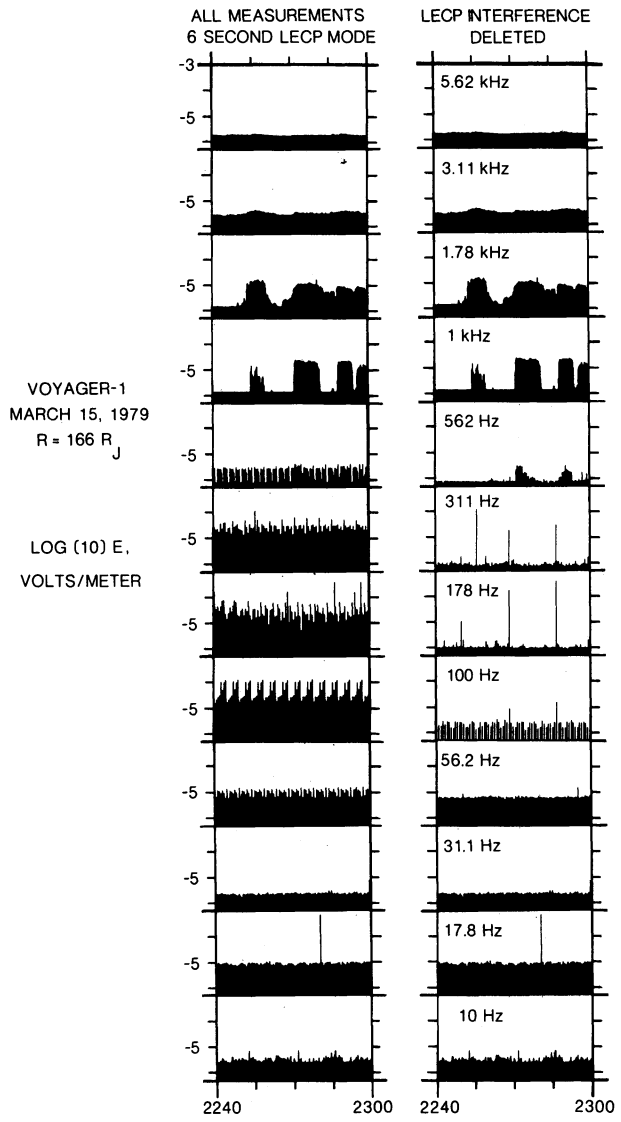

Fig. 11. Elimination of LECP stepper motor interference. The drawing on the left shows all measured points for 12 channels during a 20-min interval near 166 R_J as Voyager 1 crossed the boundary layer-magnetosphere interface. At this time the LECP instrument was stepping at its maximum 6-s rate. The drawing on the right shows the bandpass channel data reprocessed by using a computer algorithm that removes the LECP interference.

terference is predictable, we have been able to develop computer algorithms that delete all the bandpass channel points affected by the LECP. Figure 11 shows a Voyager 1 case for which the unmodified bandpass channel measurements were severely degraded when the LECP motor was in the 6-s stepping mode (left side); nevertheless, the reprocessed amplitude plots (right side) show that relatively low level ambient signals were measurable in the midst of the strong interference.

Another serious interference problem that developed within Jupiter's magnetosphere is shown in the Voyager 2 panels of Plate 1. As the spacecraft started to move away from the planet on July 10, the low-frequency levels went down in all channels except the 311-Hz channel, and Plate 1 shows that this channel had a high and steady response out to $R \simeq 200\ R_J$ on July 28. Figure 12 shows some pre- and post-encounter wideband frequency-time diagrams that reveal how the interference after July 10 involved the presence of narrow tones with f near 300 Hz. It has been determined that the serious low-frequency noise problems that developed after Voyager 2 closest approach were produced by specific gyros in the spacecraft attitude control system. The abrupt end of the intense 311-Hz noise on July 28 involved a switch to another set of gyros.

The origins of these variable interference effects are all quite mysterious at present, but the discussion shows (a) that some very definite changes developed as the Voyager spacecraft encountered Jupiter, and (b) that the wideband data link provides the only realistic way to search for the origin of the noise and the patterns of the variations.

CONCLUSIONS

The plasma wave instruments on Voyager 1 and 2 operated flawlessly during the Jupiter encounters, and they acquired an enormous amount of new information on wave-particle interactions and electromagnetic radiation of importance with respect to magnetospheric dynamics. The anticipated whistler mode turbulence was detected, the levels were measured, and the observations were used to evaluate trapped particle lifetimes and precipitation fluxes [*Scarf et al.*, 1979*b*; *Thorne and Tsurutani*, 1979; *Coroniti et al.*, 1980]. The anticipated continuum radiation was also detected, and the measurements were used to evaluate the electron density profiles [*Scarf et al.*, 1979*a*; *Gurnett et al.*, 1979*b*, 1980, 1981*a*].

The plasma wave amplitudes were found to be moderate, and the attenuators never had to be inserted, although a few intense E fields with peaks near saturation were detected. The relatively low levels for the whistler mode waves observed near closest approach can be understood by considering the high densities in the Io torus. These densities lead to high values for the index of refraction n, and since $E = cB/n$, the high n values yield moderate E fields, even though the wave energy density is high. The higher-frequency amplitudes in the continuum radiation spectrum were also relatively low, and the waves were not easy to detect in the close-in region ($r \lesssim 30\ R_J$) where N_e was high ($f_p \approx 5$–10 kHz). We conclude that these higher-frequency trapped or escaping radio waves would not have been detectable at all if the Voyager antenna length had been significantly shorter than 7 m.

The combination of accurate amplitude measurements from the 16-channel analyzer and high resolution (in time and frequency) from the waveform data link proved to be particularly beneficial. Jovian plasma waves that could not even have been detected or identified correctly without the high time resolution of the wideband data include lightning whistlers, structured chorus emissions, and broadband electrostatic emissions, as well as a number of impulsive interference signals. Other wave phenomena that could not be adequately studied without the continuous frequency resolution of the wideband link include the lower cutoff of the continuum radiation, upper hybrid resonance and half gyrofrequency harmonics, variable structure and drifts in the Jovian kilometric radio emissions, and certain narrow band spacecraft interference tones. We expect that the many thousands of additional wideband frames will also contain unique and extremely valuable information on wave-particle interactions at Jupiter.

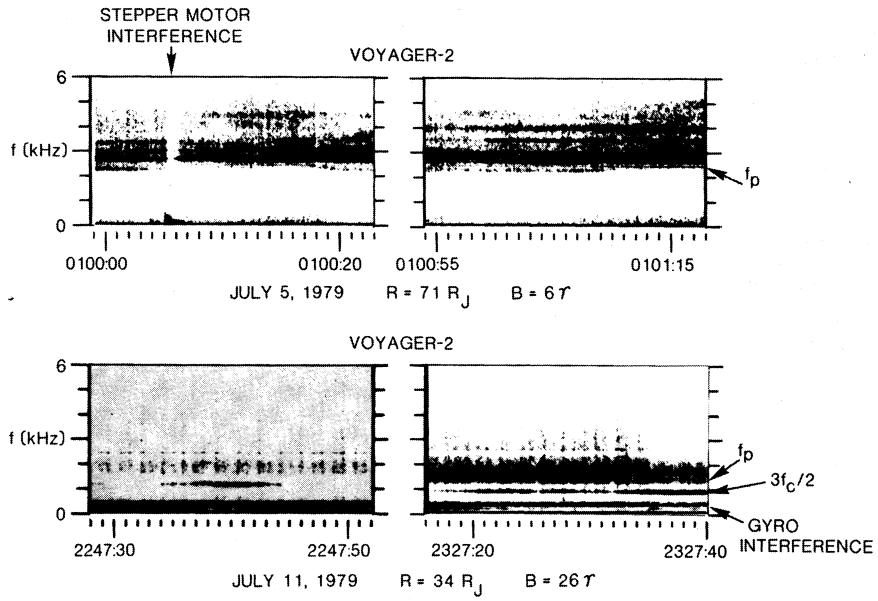

Fig. 12. Comparison of inbound and outbound wideband data from Voyager 2 that illustrates the development of a severe noise problem associated with spacecraft gyros.

Acknowledgments. We are grateful for the support we received from the Voyager Project at JPL and at NASA headquarters. We also extend our special thanks to A. Lane and R. Poynter of JPL for their efforts in improving the wideband coverage and to P. Jepsen and G. Garneau for developing the color spectrogram processing. The excellent data processing efforts of A. Cowen of TRW and the programming support provided by R. West and R. Brechwald of the University of Iowa are also gratefully acknowledged. We thank F. V. Coroniti, C. F. Kennel, S. M. Krimigis, N. F. Ness, H. Bridge, and J. Warwick for helpful discussions. The research at TRW was supported by NASA through contract 954012 with JPL. The research at the University of Iowa was supported by NASA through contract 954013 with JPL and through grant NGL-16-001-043 with NASA headquarters.

REFERENCES

Anderson, R. R., and D. A. Gurnett, Plasma wave observations near the plasmapause with the S^3–A satellite, *J. Geophys. Res.*, *78*, 4756, 1973.

Armstrong, T. P., M. T. Panessa, S. T. Brandon, S. M. Krimigis, and L. J. Lanzerotti, Low energy charged particle observations in the 5–20 R_J region of the Jovian magnetosphere, *J. Geophys. Res.*, this issue, 1981.

Bagenal, F., and J. D. Sullivan, Direct plasma measurements in the Io torus and inner magnetosphere of Jupiter, *J. Geophys. Res.*, this issue, 1981.

Barbosa, D. D., D. A. Gurnett, W. S. Kurth, and F. L. Scarf, Structure and properties of Jupiter's magnetoplasmadisc, *Geophys. Res. Lett.*, *6*, 785, 1979.

Brice, N. M., Energetic protons in Jupiter's radiation belts, Proceedings of the Workshop on Jupiter's Radiation Environment, *JPL Tech. Memo. 33-543*, 283, Jet Propul. Lab., Pasadena, Calif., 1972.

Bridge, H. S., J. W. Belcher, A. J. Lazarus, J. D. Sullivan, R. L. McNutt, F. Bagenal, J. D. Scudder, E. C. Sittler, G. L. Siscoe, V. M. Valyliunas, C. K. Goertz, and C. M. Yeates, Plasma observations near Jupiter: Initial results from Voyager 1, *Science, 204*, 987, 1979*a*.

Bridge, H. S., J. W. Belcher, A. J. Lazarus, J. D. Sullivan, F. Bagenal, R. L. McNutt, K. W. Ogilvie, J. D. Scudder, E. C. Sittler, V. M. Vasyliunas, and C. K. Goertz, Plasma observations near Jupiter: Initial results from Voyager 2, *Science*, *206*, 972, 1979*b*.

Carr, T. D. and S. Gulkis, The magnetosphere of Jupiter, *Ann. Rev. Astron. Astrophys.*, *7*, 577, 1969.

Coroniti, F. V., Denouement of Jovian radiation belt theory, in *The Magnetospheres of the Earth and Jupiter*, edited by V. Formisano, p. 391, D. Reidel, Higham, Mass., 1975.

Coroniti, F. V., R. W. Fredricks, and R. White, Instability of ring current protons beyond the plasmapause during injection events, *J. Geophys. Res.*, *77*, 6243, 1972.

Coroniti, F. V., F. L. Scarf, C. F. Kennel, W. S. Kurth, and D. A. Gurnett, Detection of Jovian whistler mode chorus: Implications for the Io torus aurora, *Geophys. Res. Lett.*, *7*, 45, 1980.

Dryer, M., Jupiter's bow shock; Comparison with theory, in *Solar Wind Three*, edited by C. T. Russell, p. 475, IUGPP (UCLA), Los Angeles, Calif., 1974.

Dryer, M., A. W. Rizzi, and W. W. Shen, Interaction of the solar wind with the outer planets, *Astrophys. Space Sci.*, *22*, 329, 1973.

Fillius, R. W., and C. E. McIlwain, Radiation belts of Jupiter, *Science*, *183*, 314, 1974.

Frank, L. A., K. L. Ackerson, J. H. Wolfe, and J. D. Mihalov, Observations of plasmas in the Jovian magnetosphere, *J. Geophys. Res.*, *81*, 457, 1976.

Goertz, C. K., Jupiter's magnetosphere: Particles and fields, in *Jupiter*, edited by T. Gehrels, p. 32, University of Arizona Press, 1976.

Goertz, C. K., Proton aurora on Jupiter's nightside, *Geophys. Res. Lett.*, *7*, 365, 1980.

Gurnett, D. A., and R. R. Shaw, Electromagnetic radiation trapped in the magnetosphere above the plasma frequency, *J. Geophys. Res.*, *78*, 8136, 1973.

Gurnett, D. A., F. L. Scarf, R. W. Fredricks, and E. J. Smith, The ISEE-1 and -2 plasma wave investigation, *Geosci. Elect.*, *GE-16*, 225, 1978.

Gurnett, D. A., R. R. Shaw, R. R. Anderson, W. S. Kurth, and F. L. Scarf, Whistlers observed by Voyager 1: Detection of lightning on Jupiter, *Geophys. Res. Lett.*, *6*, 511, 1979*a*.

Gurnett, D. A., W. S. Kurth, and F. L. Scarf, Plasma wave observations near Jupiter: Initial results from Voyager 2, *Science, 206*, 987, 1979*b*.

Gurnett, D. A., W. S. Kurth, and F. L. Scarf, The structure of the Jovian magnetotail from plasma wave observations, *Geophys. Res. Lett*, *7*, 53, 1980.

Gurnett, D. A., F. L. Scarf, W. S. Kurth, R. R. Shaw, and R. L. Poynter, Determination of Jupiter's electron density profile from plasma wave observations, *J. Geophys. Res.*, this issue, 1981*a*.

Gurnett, D. A., J. E. Maggs, D. L. Gallagher, W. S. Kurth, and F. L. Scarf, Parametric scattering and spatial collapse of beam-driven Langmuir waves in the solar wind, *J. Geophys. Res.*, this issue, 1981*b*.

Kennel, C. F., F. L. Scarf, R. W. Fredricks, J. H. McGehee, and F. V. Coroniti, VLF electric field observations in the magnetosphere, *J. Geophys. Res., 75,* 6136, 1970.

Kennel, C. F., Stably trapped proton limits for Jupiter, Proceedings of the Jupiter Radiation Belt Workshop, edited by A. J. Beck, *JPL Tech. Memo 33-543*, p. 347, Jet. Propul. Lab., Pasadena, Calif., 1972.

Krimigis, S. M., T. P. Armstrong, W. I. Axford, C. O. Bostrom, C. Y. Fan, G. Gloeckler, L. J. Lanzerotti, E. P. Keath, R. D. Zwickl, J. F. Carbary, and D. C. Hamilton, Low-energy charged particle environment at Jupiter: A first look, *Science, 204,* 998, 1979.

Kurth, W. S., D. D. Barbosa, F. L. Scarf, D. A. Gurnett, and R. L. Poynter, Low-frequency radio emissions from Jupiter: Jovian kilometric radiation, *Geophys. Res. Lett., 6,* 747, 1979.

Kurth, W. S., D. A. Gurnett, and F. L. Scarf, Spatial and temporal studies of Jovian kilometric radiation, *Geophys. Res. Lett., 7,* 61, 1980*a*.

Kurth, W. S., D. D. Barbosa, D. A. Gurnett, and F. L. Scarf, Electrostatic waves in the Jovian magnetosphere, *Geophys. Res. Lett., 7,* 57, 1980*b*.

Kurth, W. S., D. A. Gurnett, F. L. Scarf, R. L. Poynter, J. Sullivan, and H. S. Bridge, Voyager observations of Jupiter's distant magnetotail, *J. Geophys. Res.*, this issue, 1981.

Menietti, J. D., and D. A. Gurnett, Whistler propagation in the Jovian magnetosphere, *Geophys. Res. Lett., 7,* 49, 1980.

Sandel, W. R., D. E. Shemansky, A. L. Broadfoot, J. L. Bertaux, J. E. Blamont, M. J. F. Belton, J. Ajello, L. B. Holberg, J. K. Atreya, T. M. Donahue, H. W. Moss, D. F. Strobel, J. C. McConnel, A. Dalgarno, R. Goody, M. B. McElroy, and R. Takacs, Extreme ultraviolet observations from Voyager 2 encounter with Jupiter, *Science, 206,* 962, 1979.

Scarf, F. L., The magnetosphere of Jupiter and Saturn, in *The Magnetospheres of the Earth and Jupiter,* edited V. Formisano, p. 433, D. Reidel, Hingham, Mass., 1975.

Scarf, F. L., Plasma physics and wave-particle interactions at Jupiter, in *Jupiter,* edited by T. Gehrels, p. 870, University of Arizona Press, 1976.

Scarf, F. L., Plasma physics phenomena in the outer planet magnetospheres (AIAA Pap. 73-566), in *Exploration of the Outer Solar System,* edited by E. W. Greenstadt, M. Dryer, and D. S. Intriligator, p. 50, American Institute of Aeronautics and Astronautics, New York, 1977.

Scarf, F. L., and D. A. Gurnett, A plasma wave investigation for the Voyager mission, *Space Sci. Rev., 21,* 289, 1977.

Scarf, F. L., D. A. Gurnett, and W. S. Kurth, Jupiter plasma wave observations: An initial Voyager 1 overview, *Science, 204,* 991, 1979*a*.

Scarf, F. L., F. V. Coroniti, D. A. Gurnett, and W. S. Kurth, Pitch-angle diffusion by whistler mode waves near the Io plasma torus, *Geophys. Res. Lett., 6,* 653, 1979*b*.

Scarf, F. L., D. A. Gurnett, W. S. Kurth, and R. L. Poynter, Plasma wave turbulence at Jupiter's bow shock, *Nature, 280,* 796, 1979*c*.

Shaw, R. R., and D. A. Gurnett, Electrostatic noise bands associated with the electron gyrofrequency and plasma frequency in the outer magnetosphere, *J. Geophys. Res., 80,* 4259, 1975.

Smith, E. J., L. Davis, Jr., D. E. Jones, P. J. Coleman, Jr., D. S. Colburn, P. Dyal, C. P. Sonett, and A. M. A. Frandsen, The planetary magnetic field and magnetosphere of Jupiter, *J. Geophys. Res., 79,* 3501, 1974.

Thomsen, M. F., C. K. Goertz, and J. A. Van Allen, On determining magnetospheric diffusion coefficients from the observed effects of Jupiter's satellite Io, *J. Geophys. Res., 82,* 5541, 1977.

Thorne, R. M., and F. V. Coroniti, A self-consistent model for Jupiter's radiation belts, Proceedings of the Workshop on Jupiter's Radiation Environment, *JPL Tech. Memo. 33-543,* p. 363, 1972.

Thorne, R. T., and B. T. Tsurutani, Diffuse Jovian aurora influenced by plasma injection from Io, *Geophys. Res. Lett., 6,* 649, 1979.

Warwick, J. W., Particles and fields near Jupiter, *NASA CR-1685,* 1970.

Warwick, J. W., J. B. Pearce, A. C. Riddle, J. K. Alexander, M. D. Desch, M. L. Kaiser, J. R. Thieman, T. D. Carr, S. Gulkis, A. Boischot, C. C. Harvey, and B. M. Pederson, Voyager 1 planetary radio astronomy observations near Jupiter, *Science, 204,* 995, 1979.

(Received June 25, 1980;
revised October 27, 1980;
accepted October 29, 1980.)